An Improved Formulation for Structural Optimization of Nonlinear Dynamic Response

Dou, Suguang

Published in:
Advances in Nonlinear Dynamics: Proceedings of the Second International Nonlinear Dynamics Conference (NODYCON 2021)

Link to article, DOI:
10.1007/978-3-030-81162-4_38

Publication date:
2022

Document Version
Early version, also known as pre-print

An improved formulation for structural optimization of nonlinear dynamic response

Suguang Dou

DTU Wind Energy, Technical University of Denmark, Frederiksborgvej 399, 4000 Roskilde, Denmark
sudou@dtu.dk

Abstract. Nonlinear dynamics is widely exploited in micro-mechanical resonators with a number of applications. One of the crucial issues in these applications is to intentionally tailor the intrinsic nonlinearity in these structures. In this study, a structural optimization methodology is improved for tailoring the intrinsic nonlinearity in these resonators by manipulating their structural geometry. In the optimization, the objective function is defined based on the nonlinear modal coupling coefficients as well as eigenfrequencies and modal shapes of the vibration modes. A preliminary study shows that the improved formulation of the optimization problem enables better designs.

Keywords: Nonlinear dynamics, Shape optimization, Finite element, Model order reduction, Adjoint method

1 Introduction

Nonlinear dynamics has been widely exploited in a wide range of applications concerning nonlinear micro-mechanical resonators [1]. Their applications include atomic force microscopy [2], micro-mass sensors [3,4], micro-gyroscope [5], gravimeter [6], frequency division [7], and vibration energy harvester [8].

In recent years, there has been growing interest in the intentional design of nonlinearity for the purpose of tailoring the dynamic response. Many studies have investigated the applications of the shaped finger for comb drives. A few studies have applied the structural optimization techniques to tailor the mechanical nonlinearity, see e.g. [9,10,11,12,13]. In these studies, numerical optimization techniques were applied to tailor different aspects of the nonlinear dynamic responses, for example, the frequency-amplitude dependence or frequency-energy dependence [9,10], the nonlinear forced resonances [11], and the internal resonances [12,13].

In our previous study in [14], we proposed an efficient finite element based methodology for structural optimization of nonlinear micro-mechanical resonators with geometric nonlinearity described by Green stain. Later, the optimized designs were validated by using dynamic tests [15]. The fast optimization is achieved by using a direct finite element calculation of the nonlinear modal coupling coefficients [16,14]. These nonlinear modal coupling coefficients can also be

computed by using non-intrusive approaches [17]. When the structural geometry changes, these nonlinear modal coupling coefficients change accordingly, which further determine the change of the nonlinear dynamic response. The aim of this paper is to present an improved formulation for the optimization of nonlinear dynamic response through the nonlinear modal coupling coefficients.

2 Methods

The original methodology was proposed in [14] for the single-mode resonators and the multi-mode resonators with internal resonances. The methodology consists of nonlinear finite element modelling, eigenvalue analysis, direct finite element calculation of nonlinear modal coupling coefficients, and solving an optimization problem.

For brevity, the following description of the methodology is restricted to a single-mode beam resonator and its fundamental flexural mode whose eigenfrequency and eigenmode are denoted as ω and $\mathbf{\Phi}$, respectively.

2.1 Finite element model and design variables

The beam structure is discretized into a number of Euler-Bernoulli beam elements. In the optimization, the distribution of the in-plane width h of the beam is manipulated to tailor the nonlinear dynamic response, see Fig. 1. In order to ensure the effectiveness of the Euler-Bernoulli beam element, it is assumed that the distribution of the in-plane width varies continuously without drastic change. For the purpose of optimization, a large number of elements are used to enable a fine representation of the varying in-plane width . In order to ensure

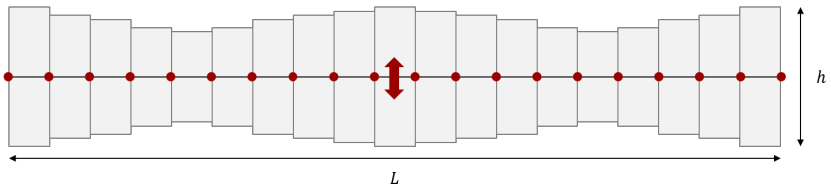

Fig. 1. Illustration of the varying in-plane width, the beam elements, and the direction of the in-plane vibration.

manufacturability and mechanical strength, it is reasonable to impose a lower bound h_{min} on the in-plane width. On the other hand, an upper bound h_{max} is also imposed on the in-plane width to suit the applicability of the beam theory. With the lower and upper bounds of the in-plane width, the design variables are defined as

$$h_e = h_{min} + \rho_e(h_{max} - h_{min}) \tag{1}$$

where $e = 1, \ldots, N_e$ with N_e denoting the number of the beam elements.

2.2 Reduced-order model and frequency-amplitude relation

Assume that the flexural vibration of the beam in its fundamental mode can be approximated by $\mathbf{u} = x\,\mathbf{\Phi}$ with $\mathbf{u}$ denoting the full-order displacement vector. The reduced-order model of the beam in its fundamental mode is described by the standard Duffing equation as follows

$$\ddot{x} + 2\,\xi\,\omega\,\dot{x} + \omega^2 x + \alpha\,x^3 = f\cos(\Omega\,t) \tag{2}$$

where ξ is the modal damping ratio, ω is the eigen-frequency of the vibration mode, α is the coefficient of the cubic nonlinear stiffness term (Duffing nonlinearity), f and Ω are the amplitude and frequency of the external force, respectively. The eigen-frequency ω is obtained by solving an eigenvalue problem

$$\mathbf{K}\mathbf{\Phi} = \omega^2\mathbf{M}\mathbf{\Phi} \tag{3}$$

where $\mathbf{M}$ and $\mathbf{K}$ are the mass matrix and the stiffness matrix in the finite element model. Further, the eigen-mode is normalized with respect to the mass matrix, i.e.

$$\mathbf{\Phi}^T\mathbf{M}\mathbf{\Phi} = 1 \tag{4}$$

In the reduced-order model in Eq. (2), the coefficient of the cubic nonlinearity is directly calculated in the finite element model as [14]

$$\alpha = 4\sum_{e=1}^{N_e}\frac{EA(\rho_e)}{8L}\left(\mathbf{w}_e(\boldsymbol{\rho})^{\mathrm{T}}\mathbf{K}_g\mathbf{w}_e(\boldsymbol{\rho})\right)^2 \tag{5}$$

where $\mathbf{w}_e$ denotes an element-wise vector taken from the vibration mode $\mathbf{\Phi}$ corresponding to the deflection of the beam element e. The matrix $\mathbf{K}_g$ is given as [18]

$$\mathbf{K}_g = \frac{1}{30\,l}\begin{bmatrix} 36 & 3l & -36 & 3l \\ 3l & 4l^2 & -3l & -l^2 \\ -36 & -3l & 36 & -3l \\ 3l & -l^2 & -3l & 4l^2 \end{bmatrix} \tag{6}$$

where l is the length of the beam element e.

Note that Eq. (5) is derived for beam element with the nonlinearity arising from the mid-plane stretching effect existing in clamped-clamped beam and similar beam structures. This mid-plane stretching effect is not suitable to cantilever beam whose length can be seen as non-extensible. Alternatively, Eq. (5) can also be derived for the solid element with Green strain [14] which has a wider applicability.

The frequency of the resonance peak increases as the amplitude of the resonance peak increases, which is described as

$$\omega_p = \omega(1 + \gamma A_p^2) \tag{7}$$

where ω_p and A_p denote the frequency and amplitude of the nonlinear forced resonance peak, respectively. The effective coefficient γ is given as

$$\gamma = \frac{3}{8}\frac{\alpha}{\omega^2} \tag{8}$$

It is emphasized that in the above derivation of γ can not fully reflect the change of the magnitude of the vibration mode $\mathbf{\Phi}$, and thus may to some extent bias the optimized design in the optimization as shown later in the numerical results.

In order to account for the change of the magnitude of the vibration mode, let $|\mathbf{\Phi}|$ denote the magnitude of the vibration mode, and introduce a new coordinate $y = x\,|\mathbf{\Phi}|$. The change of the coordinate from x to y corresponds to a change of the reduction basis from $\mathbf{\Phi}$ to $\frac{\mathbf{\Phi}}{|\mathbf{\Phi}|}$. The reduced-order model in Eq. (2) can be re-written as

$$\ddot{y} + 2\xi\omega\dot{y} + \omega^2 y + \beta y^3 = g\cos\omega t \tag{9}$$

where

$$y = x\,|\mathbf{\Phi}|, \quad \beta = \frac{\alpha}{|\mathbf{\Phi}|^2}, \quad g = f\,|\mathbf{\Phi}| \tag{10}$$

For the fundamental vibration mode of the clamped-clamped beam, its magnitude can be captured by the deflection at the midspan as

$$|\mathbf{\Phi}| = \max(\mathbf{\Phi}) = |\mathbf{L}^T\mathbf{\Phi}| \tag{11}$$

where $\mathbf{L}$ is a vector with all zeros but one non-zero component. The value of the non-zero component is one. Its index corresponds to the degree of freedom of the maximum deflection at the midspan of the beam.

From the reduced-order model in Eq. (9), the frequency-amplitude relation can be re-written as

$$\omega_p = \omega(1 + \mathit{\Gamma} B_p^2) \tag{12}$$

where B_p is the amplitude of the resonance peak in the coordinate of y, and the effective coefficient $\mathit{\Gamma}$ is given as

$$\mathit{\Gamma} = \frac{3}{8}\frac{\beta}{\omega^2} = \frac{3}{8}\frac{\alpha}{\omega^2\,|\mathbf{\Phi}|^2} = \frac{\gamma}{|\mathbf{\Phi}|^2} \tag{13}$$

The effective coefficient in Eq. (13) is derived in the coordinate of y and the reduction basis $\frac{\mathbf{\Phi}}{|\mathbf{\Phi}|}$. Since the new reduction basis is normalized with its magnitude, the resulting effective coefficient $\mathit{\Gamma}$ provides a fair comparison of the optimized designs in the numerical computation. This also implies that an alternative way to account for the change of the magnitude of the eigenmode is to use the eigenmode that is normalized with its magnitude. Specifically, one can replace Eq. (4) with

$$|\mathbf{\Phi}_i| = 1 \tag{14}$$

In the following formulation and the numerical results, the normalization of the eigenmode with respect to the mass matrix in Eq. (4) is used, and the two effective coefficients in Eq. (13) and Eq. (8) are compared in the context of optimization.

2.3 Optimization problems and sensitivities

First, the original formulation of the optimization problem to maximize the hardening behavior of a clamped-clamped beam resonator is

$$\begin{aligned} \max_{\boldsymbol{\rho}} \quad & \overline{\gamma} = \frac{\alpha}{\omega^2} \\ \text{subject to:} \quad & (\mathbf{K} - \omega^2 \mathbf{M})\boldsymbol{\Phi} = \mathbf{0}, \\ & \boldsymbol{\Phi}^T \mathbf{M} \boldsymbol{\Phi} = 1, \\ & V(\boldsymbol{\rho})/V^* \leq 0.5, \\ & \mathbf{0} \leq \boldsymbol{\rho} \leq \mathbf{1}. \end{aligned} \tag{P_{old}}$$

where the new objective function is defined in terms of γ in Eq. (8), and the constant factor $\frac{3}{8}$ is omitted in the objective function.

Based on the above formulation, the improved formulation of the same optimization problem is written as

$$\max_{\boldsymbol{\rho}} \quad \overline{\Gamma} = \frac{\alpha}{\omega^2 \left|\boldsymbol{\Phi}\right|^2} \tag{P_{new}}$$

where the objective function is defined in terms of Γ in Eq. (13), and the constraints are the same as those in the problem P_{new} and therefore are omitted.

The two optimization problems are solved by using a gradient-based optimizer called the Method of Moving Asymptotes (MMA) [20], which is efficient and robust for solving structural optimization problems. The design sensitivities (i.e. gradients) of the objective functions with respect to the design variables are calculated by using the adjoint method [19] as described in the following subsection.

2.4 Design sensitivity analysis using the adjoint method

The derivation of the design sensitivity analysis is demonstrated by using the new objective function $\overline{\Gamma}$ in P_{new}.

First, two adjoint variables, $\boldsymbol{\lambda}$ and η, are introduced in order to apply the adjoint method in the design sensitivity analysis. The objective function is rewritten as

$$\overline{\Gamma} = \overline{\Gamma} + \boldsymbol{\lambda}^T \left(\mathbf{K} - \omega^2 \mathbf{M}\right) \boldsymbol{\Phi} + \eta \left(\boldsymbol{\Phi}^T \mathbf{M} \boldsymbol{\Phi} - 1\right) \tag{15}$$

The gradients of the augmented objective function are derived as

$$\begin{aligned}\frac{\mathrm{d}\overline{\Gamma}}{\mathrm{d}\rho_e} &= \frac{\partial\overline{\Gamma}}{\partial\omega}\frac{\mathrm{d}\omega}{\mathrm{d}\rho_e} + \frac{\partial\overline{\Gamma}}{\partial\alpha}\left(\frac{\partial\alpha}{\partial\rho_e} + \frac{\partial\alpha}{\partial\boldsymbol{\Phi}}\frac{\mathrm{d}\boldsymbol{\Phi}}{\mathrm{d}\rho_e}\right) + \frac{\partial\overline{\Gamma}}{\partial|\boldsymbol{\Phi}|}\frac{\partial|\boldsymbol{\Phi}|}{\partial\boldsymbol{\Phi}}\frac{\mathrm{d}\boldsymbol{\Phi}}{\mathrm{d}\rho_e} \\ &+ \boldsymbol{\lambda}^T\left[\left(\frac{\partial\mathbf{K}}{\partial\rho_e} - \omega^2\frac{\partial\mathbf{M}}{\partial\rho_e}\right)\boldsymbol{\Phi} - 2\omega\mathbf{M}\boldsymbol{\Phi}\frac{\mathrm{d}\omega}{\mathrm{d}\rho_e} + \left(\mathbf{K} - \omega^2\mathbf{M}\right)\frac{\mathrm{d}\boldsymbol{\Phi}}{\mathrm{d}\rho_e}\right] \\ &+ \eta\left(\boldsymbol{\Phi}^T\frac{\partial\mathbf{M}}{\partial\rho_e}\boldsymbol{\Phi} + 2\,\boldsymbol{\Phi}^T\mathbf{M}\frac{\mathrm{d}\boldsymbol{\Phi}}{\mathrm{d}\rho_e}\right)\end{aligned} \tag{16}$$

Collecting the terms of $\frac{\mathrm{d}\boldsymbol{\Phi}}{\mathrm{d}\rho_e}$ and $\frac{\mathrm{d}\omega}{\mathrm{d}\rho_e}$, we have

$$\begin{aligned}\frac{\mathrm{d}\overline{\Gamma}}{\mathrm{d}\rho_e} &= \frac{\partial\overline{\Gamma}}{\partial\alpha}\frac{\partial\alpha}{\partial\rho_e} + \boldsymbol{\lambda}^T\left(\frac{\partial\mathbf{K}}{\partial\rho_e} - \omega^2\frac{\partial\mathbf{M}}{\partial\rho_e}\right)\boldsymbol{\Phi} + \eta\,\boldsymbol{\Phi}^T\frac{\partial\mathbf{M}}{\partial\rho_e}\boldsymbol{\Phi} \\ &+ \left(\frac{\partial\overline{\Gamma}}{\partial\alpha}\frac{\partial\alpha}{\partial\boldsymbol{\Phi}} + \frac{\partial\overline{\Gamma}}{\partial|\boldsymbol{\Phi}|}\frac{\partial|\boldsymbol{\Phi}|}{\partial\boldsymbol{\Phi}} + \boldsymbol{\lambda}^T\left(\mathbf{K} - \omega^2\mathbf{M}\right) + 2\,\eta\,\boldsymbol{\Phi}^T\mathbf{M}\right)\frac{\mathrm{d}\boldsymbol{\Phi}}{\mathrm{d}\rho_e} \\ &+ \left(\frac{\partial\overline{\Gamma}}{\partial\omega} + \boldsymbol{\lambda}^T(-2\omega\mathbf{M}\boldsymbol{\Phi})\right)\frac{\mathrm{d}\omega}{\mathrm{d}\rho_e}\end{aligned} \tag{17}$$

The values of the two adjoint variables can be chosen so that the two terms of $\frac{\mathrm{d}\boldsymbol{\Phi}}{\mathrm{d}\rho_e}$ and $\frac{\mathrm{d}\omega}{\mathrm{d}\rho_e}$ vanish in the above equation, leading to a set of adjoint equations as

$$\begin{aligned}\frac{\partial\overline{\Gamma}}{\partial\alpha}\frac{\partial\alpha}{\partial\boldsymbol{\Phi}} + \frac{\partial\overline{\Gamma}}{\partial|\boldsymbol{\Phi}|}\frac{\partial|\boldsymbol{\Phi}|}{\partial\boldsymbol{\Phi}} + \boldsymbol{\lambda}^T\left(\mathbf{K} - \omega^2\mathbf{M}\right) + 2\,\eta\,\boldsymbol{\Phi}^T\mathbf{M} &= \mathbf{0} \\ \frac{\partial\overline{\Gamma}}{\partial\omega} + \boldsymbol{\lambda}^T(-2\omega\mathbf{M}\boldsymbol{\Phi}) &= 0\end{aligned} \tag{18}$$

The adjoint equations can be re-formulated into matrix form as

$$\begin{bmatrix}\mathbf{K} - \omega^2\mathbf{M} & 2\,\boldsymbol{\Phi}^T\mathbf{M} \\ 2\,\boldsymbol{\Phi}^T\mathbf{M} & 0\end{bmatrix}\begin{bmatrix}\boldsymbol{\lambda} \\ \eta\end{bmatrix} = \begin{bmatrix}-\frac{\partial\overline{\Gamma}}{\partial\alpha}\frac{\partial\alpha}{\partial\boldsymbol{\Phi}} - \frac{\partial\overline{\Gamma}}{\partial|\boldsymbol{\Phi}|}\frac{\partial|\boldsymbol{\Phi}|}{\partial\boldsymbol{\Phi}} \\ \frac{1}{\omega}\frac{\partial\overline{\Gamma}}{\partial\omega}\end{bmatrix} \tag{19}$$

After solving the adjoint equations (19), the adjoint variables $\boldsymbol{\lambda}$ and η are determined. Then the sensitivities of the objective function are calculated as

$$\frac{\mathrm{d}\overline{\Gamma}}{\mathrm{d}\rho_e} = \frac{\partial\overline{\Gamma}}{\partial\alpha}\frac{\partial\alpha}{\partial\rho_e} + \boldsymbol{\lambda}^T\left(\frac{\partial\mathbf{K}}{\partial\rho_e} - \omega^2\frac{\partial\mathbf{M}}{\partial\rho_e}\right)\boldsymbol{\Phi} + \eta\,\boldsymbol{\Phi}^T\frac{\partial\mathbf{M}}{\partial\rho_e}\boldsymbol{\Phi} \tag{20}$$

When the given values of the adjoint variables $\boldsymbol{\lambda}$ and η, the right-hand side of Eq. (20) is cheap to compute for all design variables.

In each optimization iteration, the adjoint equations in Eq. (19) only need to be solved once and then the resulting values of the adjoint variables $\boldsymbol{\lambda}$ and η can be used in Eq. (20) to compute the sensitivities of the objective function with respect to all the design variables ρ_e with $e = 1, \ldots, N_e$.

The adjoint method is more efficient than the direct differentiation method and the numerical finite difference approximation of the sensitivities, and thus allows a large number of design variables to be used in the optimization.

For the optimization problem P_{old}, the adjoint equations and the sensitivities of the objective function are given as

$$\begin{bmatrix} \mathbf{K} - \omega^2 \mathbf{M} & 2\,\mathbf{\Phi}^T \mathbf{M} \\ 2\,\mathbf{\Phi}^T \mathbf{M} & 0 \end{bmatrix} \begin{bmatrix} \boldsymbol{\lambda} \\ \eta \end{bmatrix} = \begin{bmatrix} -\frac{\partial \overline{\gamma}}{\partial \alpha} \frac{\partial \alpha}{\partial \mathbf{\Phi}} \\ \frac{1}{\omega} \frac{\partial \overline{\Gamma}}{\partial \omega} \end{bmatrix} \tag{21}$$

$$\frac{\mathrm{d}\overline{\gamma}}{\mathrm{d}\rho_e} = \frac{\partial \overline{\gamma}}{\partial \alpha} \frac{\partial \alpha}{\partial \rho_e} + \boldsymbol{\lambda}^T \left(\frac{\partial \mathbf{K}}{\partial \rho_e} - \omega^2 \frac{\partial \mathbf{M}}{\partial \rho_e} \right) \mathbf{\Phi} + \eta\, \mathbf{\Phi}^T \frac{\partial \mathbf{M}}{\partial \rho_e} \mathbf{\Phi} \tag{22}$$

3 Results

The improved optimization is applied to a micro-mechanical clamped-clamped beam in [14]. The evolution of the design is displayed in Fig. 2. The vibration mode of the final design is displayed in Fig. 3. For comparison, the old design and its fundamental flexural mode are displayed in Fig. 4.

Fig. 2 shows that in the first 10 iterations, the optimizer distributes more material at two locations where the nonlinear strain energy is high [11]. In the following iterations, the optimizer begins to put more material at the midspan of the beam, yielding a central mass. The central mass was not shown in the design by using the original approach [14] and therefore is attributed to the improved optimization. Its occurrence is attributed to the improvement in the methodology, i.e. the change of the magnitude of the vibration mode is taken into account. The occurrence of central mass coincides with the fact that a central mass is used in ultra-wide bandwidth piezoelectric energy harvesting devices [8] and another result in topology optimization [21].

Further study is required to the applicability of the improved formulation of the optimization problem in a wider range of applications.

Table 3 shows a comparison of the two designs obtained by using the original objective function in P_{old} and the improved objective function in P_{new}. Note that γ_0 and Γ_0 are the corresponding values of the same initial design, while γ and Γ are the corresponding values of the two final designs. According to $\frac{\Gamma}{\Gamma_0}$, the new design obtained by using P_{new} has a larger value of Γ than the old design obtained by using P_{old}. However, when using the objective function based on γ, this new design is a sub-optimal design because of the bias of the objective function. As discussed in Section 2 concerning the reduced-order models and frequency-amplitude relation, Γ provides a fair comparison of the optimized designs. This new design has a larger value of Γ. Consequently, this new design has a larger frequency shift for a given amplitude of the resonant peak than the old design. The improvement obtained by using the improved formulation in this example is 6.4%. In future work the two optimized designs will be compared by using nonlinear frequency response and ring-down response.

4 Conclusions

This paper presents an improved formulation of the optimization problem for tuning the nonlinear dynamic response through the nonlinear modal coupling

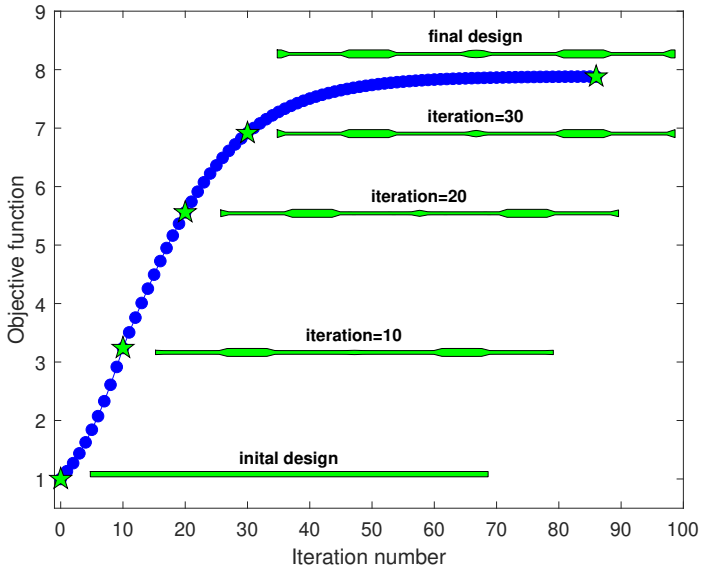

Fig. 2. The optimized design for maximizing the hardening behavior of the fundamental vibration mode of a clamped-clamped beam resonator. The objective function is normalized with its value of the initial design.

Fig. 3. The fundamental flexural mode the new design for maximizing the hardening behavior of a clamped-clamped beam. The color denotes the total displacement. The mode shape is obtained by using COMSOL Multiphysics 5.4 with 2D solid element.

Fig. 4. The fundamental flexural mode of the design in [14] for maximizing the hardening behavior of a clamped-clamped beam . The color denotes the total displacement. The mode shape is obtained by using COMSOL Multiphysics 5.4 with 2D solid element. The image is re-used from [14].

coefficients. For the hardening behavior of a clamped-clamped beam, the design obtained by using the improved formulation has a larger effective coefficient Γ than the design obtained by using the original formulation.

Further studies are required to extend this improved formulation of the optimization problem to multi-mode micro-mechanical resonators [14], topology optimization [21,22], and optimization problems of micro-mechanical resonators with electrostatic actuation [23]. Additional studies are needed to examine the

Table 1. Comparison the two designs obtained by using the original objective function in P_{old} and the improved objective function in P_{new}.

	P_{old}	P_{new}	ratio
$\frac{\gamma}{\gamma_0}$	13.35	10.11	0.757
$\frac{\Gamma}{\Gamma_0}$	7.56	8.05	1.064

potential extension of the optimization frame to micro-mechanical cantilever-based structures with nonlinear inertial effects and nano-mechanical resonators where the non-local elastic effects prevail in the nonlinearity [24].

References

1. Rhoads, J.F., Shaw, S.W., Turner, K.L.: Nonlinear dynamics and its applications in micro- and nanoresonators. J. Dyn. Syst., Meas., Control **132**, 034001 (2010)
2. Jeong, B., Pettit, C., Dharmasena, S., Keum, H., Lee, J., Kim, J., Kim, S., McFarland, D.M., Bergman, L.A., Vakakis, A.F., Cho, H.: Utilizing intentional internal resonance to achieve multi-harmonic atomic force microscopy. Nanotechnology **27**, 125501 (2016)
3. Zhang, W., Baskaran, R., Turner, K.L.: Effect of cubic nonlinearity on auto-parametrically amplified resonant MEMS mass sensor. Sens. Actuator A Phys. 102 139–150 (2002)
4. Meesala, V.C., Hajj, M.R. and Abdel-Rahman, E.: Bifurcation-based MEMS mass sensors. Int. J. Mech. Sci. **180**, 105705 (2020)
5. Nitzan, S.H., Zega, V., Li, M., Ahn, C.H., Corigliano, A., Kenny, T.W., Horsley, D.A.: Self-induced parametric amplification arising from nonlinear elastic coupling in a micromechanical resonating disk gyroscope. Sci. Rep. **5** 9036 (2015)
6. Middlemiss, R.P., Samarelli, A., Paul, D.J., Hough, J., Rowan, S., Hammond, G.D.: Measurement of the Earth tides with a MEMS gravimeter. Nature **531** 614–617 (2016)
7. Qalandar, K.R., Strachan, B.S., Gibson, B., Sharma, M., Ma, A., Shaw, S.W., Turner, K.L.: Frequency division using a micromechanical resonance cascade. Appl. Phys. Lett. **105**, 244103 (2014)
8. Hajati, A., Kim, S.G.: Ultra-wide bandwidth piezoelectric energy harvesting. *Appl. Phys. Lett.* **99**, 083105 (2011)
9. Dou, S., Jensen, J.S.: Optimization of hardening/softening behavior of plane frame structures using nonlinear normal modes. Computers Structures **164**, 63–74 (2016)
10. Detroux, T., Noël, J., Kerschen, G.: Tailoring the resonances of nonlinear mechanical systems. Nonlinear Dyn. (2020) https://doi.org/10.1007/s11071-020-06002-w
11. Dou, S., Jensen, J.S.: Optimization of nonlinear structural resonance using the incremental harmonic balance method. J. Sound Vib. **334**, 239–54 (2015)
12. Tripathi, A., Bajaj, A.K.: Computational synthesis for nonlinear dynamics based design of planar resonant structures. J. Vib. Acoust. **135**, 051031 (2013)
13. Tripathi, A., Bajaj, A.K.: Topology optimization and internal resonances in transverse vibrations of hyperelastic plates. Int. J. Solids Struct. **81**, 311–328 (2016)

14. Dou, S., Strachan, B.S., Shaw, S.W., Jensen, J.S.: Structural optimization for nonlinear dynamic response. Phil. Trans. R. Soc. A **373**, 20140408 (2015)
15. Li, L.L., Polunin, P.M., Dou, S., Shoshani, O., Strachan, B.S., Jensen, J.S., Shaw, S.W., Turner, K.L.: Tailoring the nonlinear response of MEMS resonators using shape optimization. Appl. Phys. Lett. **110**, 081902 (2017)
16. Touzé, C., Vidrascu, M., Chapelle, D.: Direct finite element computation of nonlinear modal coupling coefficients for reduced-order shell models. Comput. Mech. **54**: 567–580 (2014)
17. Frangi, A., Gobat, G.: Reduced order modelling of the non-linear stiffness in MEMS resonators. Int. J. Non Linear Mech. **116**, 211–218 (2019)
18. Chen, S.H., Cheung, Y.K., Xing, H.X.: Nonlinear vibration of plane structures by finite element and incremental harmonic balance method. Nonlinear Dyn. **26**, 87–104 (2001)
19. Van Keulen, F., Haftka, R.T., Kim, N.H.: Review of options for structural design sensitivity analysis. Part 1: Linear systems. Comput. Methods in Appl. Mech. Eng. **194**, 3213–3243 (2005)
20. Svanberg, K.: The method of moving asymptotes–a new method for structural optimization. Int. J. Numer. Methods Eng. **24**, 359–373 (1987)
21. Dou, S., Jensen, J.S.: Analytical sensitivity analysis and topology optimization of nonlinear resonant structures with hardening and softening behavior. In: 17th U.S. National Congress on Theoretical and Applied Mechanics, East Lansing (2014) https://orbit.dtu.dk/en/publications/analytical-sensitivity-analysis-and-topology-optimization-of-nonl
22. Jensen, J.S., Dou, S.: Topology optimization in nonlinear structural dynamics using direct computation of nonlinear coefficients. In: ECCOMAS Congress 2016: VII European Congress on Computational Methods in Applied Sciences and Engineering, Crete (2016) https://orbit.dtu.dk/en/publications/topology-optimization-in-nonlinear-structural-dynamics-using-dire
23. Jensen, J.S., Dou, S., Shaw, S.W.: Tailoring nonlinear dynamics of microbeam resonators with electrostatic actuation. In: Proceeding of 24th International Congress of Theoretical and Applied Mechanics, vol. 1, pp. 148–149 (2016) https://orbit.dtu.dk/en/publications/tailoring-nonlinear-dynamics-of-microbeam-resonators-with-electro
24. Eltaher, M.A., Khater M.E., Emam S.A.: A review on nonlocal elastic models for bending, buckling, vibrations, and wave propagation of nanoscale beams. Appl. Math. Model. **40** 4109–4128 (2016)